# The Tropical Cyclone Diurnal Cycle of Mature Hurricanes

JASON P. DUNION

*Cooperative Institute for Marine and Atmospheric Studies, University of Miami, and Hurricane Research Division, NOAA/Atlantic Oceanographic and Meteorological Laboratory, Miami, Florida*

CHRISTOPHER D. THORNCROFT

*University at Albany, State University of New York, Albany, New York*

CHRISTOPHER S. VELDEN

*Cooperative Institute for Meteorological Satellite Studies, University of Wisconsin–Madison, Madison, Wisconsin*

(Manuscript received 7 June 2013, in final form 2 June 2014)

ABSTRACT

The diurnal cycle of tropical convection and the tropical cyclone (TC) cirrus canopy has been described extensively in previous studies. However, a complete understanding of the TC diurnal cycle remains elusive and is an area of ongoing research. This work describes a new technique that uses infrared satellite image differencing to examine the evolution of the TC diurnal cycle for all North Atlantic major hurricanes from 2001 to 2010. The imagery reveals cyclical pulses in the infrared cloud field that regularly propagate radially outward from the storm. These diurnal pulses begin forming in the storm's inner core near the time of sunset each day and continue to move away from the storm overnight, reaching areas several hundreds of kilometers from the circulation center by the following afternoon. A marked warming of the cloud tops occurs behind this propagating feature and there can be pronounced structural changes to a storm as it moves away from the inner core. This suggests that the TC diurnal cycle may be an important element of TC dynamics and may have relevance to TC structure and intensity change. Evidence is also presented showing the existence of statistically significant diurnal signals in TC wind radii and objective Dvorak satellite-based intensity estimates for the 10-yr hurricane dataset that was examined. Findings indicate that TC diurnal pulses are a distinguishing characteristic of the TC diurnal cycle and the repeatability of TC diurnal pulsing in time and space suggests that it may be an unrealized, yet fundamental TC process.

## 1. Introduction

Although numerous studies have documented the existence of diurnal maxima and minima associated with tropical oceanic convection and the tropical cyclone (TC) upper-level cirrus canopy, we lack a thorough understanding of the nature and causes of these variations and especially the extent to which these variations are important for TCs. It is well known that the coherent diurnal cycle of deep cumulus convection and associated rainfall is different over the land and ocean (Gray and Jacobson 1977; Yang and Slingo 2001). While over the land it tends to peak in the late afternoon/early evening due to daytime boundary layer heating, over the ocean it peaks in the early morning. In addition, Gray and Jacobson (1977), Mapes and Houze (1993), and Liu and Moncrieff (1998) found that the oceanic peak was more prominent when the preexisting convection was more intense and associated with an organized weather system such as an African easterly wave or mesoscale convective system. Numerous studies have also highlighted diurnal changes in the cirrus anvils of tropical deep convection and TCs. Weikmann et al. (1977) noted that anvils emanating from large cumulonimbus clouds tended to grow preferably between 2200 and 0300 local standard time (LST). Browner et al. (1977) found that the areal extent of the TC cirrus canopy was a minimum at 0300 LST and a maximum at 1700 LST and suggested that this diurnal oscillation

*Corresponding author address:* Jason P. Dunion, Rosenstiel School of Marine and Atmospheric Science, Cooperative Institute for Marine and Atmospheric Studies, University of Miami, 4600 Rickenbacker Causeway, Miami, FL 33149.
E-mail: jason.dunion@noaa.gov

DOI: 10.1175/MWR-D-13-00191.1

might be important for the TC. More recently, Kossin (2002) used storm-centered Geostationary Operational Environmental Satellite (GOES) infrared (IR) imagery to calculate azimuthally averaged brightness temperatures and create Hovmöller-type diagrams of brightness temperature diurnal oscillations over time. That study concluded that although a clear diurnal oscillation of the TC cirrus canopy was present at larger radii (e.g., 300 km), few storms exhibited diurnal oscillation signals in their innermost 100 km. It was hypothesized that different processes might be forcing periodic oscillations in the TC deep inner-core convection and the TC cirrus canopy. The present paper aims to document the TC diurnal cycle and associated diurnal pulses in mature TCs.

The current study takes a novel approach to investigating diurnal oscillations in TCs and finds an intriguing diurnal pulsing pattern that appears to occur with remarkable regularity through a relatively deep layer of the TC. Storm-centered GOES and Meteosat Second Generation (MSG) IR imagery (10.7 and 10.8 $\mu$m) were used to create 6-h brightness temperature difference fields of the storm's inner core and its surrounding environment ($R = 100$–$600$ km). The imagery reveals periodic oscillations of cooling and warming in the IR brightness temperature field over time. One prominent characteristic of these oscillations is a cold ring (i.e., local cooling of the brightness temperatures with time) that begins forming in the storm's inner core ($R \sim \leq 150$ km; Rogers et al. 2012) near the time of sunset each day. This cold ring feature (hereafter referred to as a diurnal pulse) continues to move away from the storm overnight, reaching areas several hundred kilometers from the circulation center by the following afternoon. A marked warming of the cloud tops occurs behind this propagating feature and structural changes in the storm are noted as it moves away from the inner core. This systematic variation of cloud-top temperatures suggests that diurnal pulses may have implications for TC intensity change. The current study examined all North Atlantic major hurricanes from 2001 to 2010 and findings suggest that TC diurnal pulses are a distinguishing characteristic of the TC diurnal cycle.

This manuscript is organized in the following manner: section 2 outlines the various datasets and methodology that were used to examine the TC diurnal cycle. Section 3 presents two TC case studies from the 2001–10 dataset that exhibited diurnal pulsing during their life cycles. This section also describes mean statistics of the 10-yr TC diurnal cycle dataset and presents evidence of a diurnal signal in a few parameters that describe and estimate TC structure and intensity. While the exact processes that cause the TC diurnal cycle and associated diurnal pulses remain uncertain, several hypotheses that could explain their development and evolution are posed in section 4. Although the main focus of this study is to document observational aspects and tracking capabilities of TC diurnal cycle characteristics, its remarkable predictability (timing and propagation) provides an opportunity to advance our understanding of this phenomenon in the future.

## 2. Data and methods

This study examined 3-hourly GOES 4-km IR (10.7 $\mu$m) imagery for all Atlantic major hurricanes from 2001 to 2010 and included over 850 satellite images for 36 TCs.[1] The 3-hourly image increment that was selected minimized satellite eclipse period data gaps and when images were missing, temporal discontinuities from substituted images never exceeded 30 min. Each storm-centric image was geolocated using a combination of National Hurricane Center best track data, aircraft center positions, and (when an eye was present) positions determined manually using the Man Computer Interactive Data Access System (McIDAS; Lazzara et al. 1999). Two types of storm-centered IR imagery (remapped to Mercator projection) were examined in detail: standard geostationary imagery and 6-h brightness temperature differencing imagery (i.e., IR differencing imagery). The latter was created by differencing the brightness temperature fields of two consecutive storm-centered IR images separated by 6 h and color enhanced to resemble conventional IR brightness temperature scales (i.e., warm colors represent colder cloud tops). The resulting satellite image has utility for quantifying brightness temperature changes in the TC environment and for monitoring structural changes in the TC cirrus canopy, eye, and regions of deep convection (in areas not obscured by the cirrus canopy). Azimuthal means of the IR brightness temperatures and 6-h IR brightness temperature differences (i.e., trends) were calculated every 3 h at 100-km radius intervals (100–600 km) for each storm in the 10-yr dataset. This information provided a means to monitor diurnal variations in the brightness temperature fields of the various storm environments. It should be noted that other IR brightness temperature differencing increments (e.g., 3 h) and satellite channels (e.g., the 6.5- and 6.8-$\mu$m water vapor channels) were also tested and will be investigated in more detail in the near future.

The IR satellite imagery that was used in this study typically detects high-level cirrus in the TC canopy and

[1] MSG IR imagery (10.8 $\mu$m) was used to supplement the GOES IR imagery for storms located east of 37.5°W.

embedded deep convection. Therefore, in cases of moderate-to-high shear (e.g., $>7.5\,m\,s^{-1}$), asymmetries in the observed satellite cloud field will often occur and may not necessarily reflect the typical TC outflow pattern.[2] Additionally, terrain-induced convection (e.g., related to frictional convergence and surface heating) in the periphery of TCs near land can promote convective development that may not be representative of a TC's natural convective patterns. Finally, weak or incipient TCs often exhibit sporadic and/or asymmetric convective activity that may not reflect the natural convective cycles that are inherent in mature TCs. Based on these considerations, the following criteria were used to subsample each 3-h cycle for the storms in the 10-yr dataset: 1) 200–850-hPa vertical wind shear $\leq 7.5\,m\,s^{-1}$ [determined from the Statistical Hurricane Intensity Prediction Scheme (SHIPS; DeMaria et al. 2005)]; 2) storm center ≥300 km from land;[3] and 3) Saffir–Simpson storm intensity of category 2 or higher ($\geq 43\,m\,s^{-1}$). Additionally, for each TC, a continuous 72-h period was identified that was roughly centered around the storm's peak intensity while also maximizing the number of usable azimuthal calculations. The 72-h time window was chosen based upon the fact that North Atlantic major hurricanes only maintain category 3 or higher intensity ($\geq 49\,m\,s^{-1}$) for an average of ~2.5 days (Jarvinen et al. 1984). The selection criteria described above resulted in 450 individual 3-hourly brightness temperature–brightness temperature trend azimuthal calculation sets for 31 North Atlantic major hurricanes from 2001 to 2010 (Table 1).

Microwave satellite imagery (37- and 85/89/91-GHz channels) from the National Aeronautics and Space Administration (NASA) *Aqua* Advanced Microwave Scanning Radiometer for Earth Observing System (EOS) (AMSR-E) and the Defense Meteorological Satellite Program (DMSP) microwave imagers [Special Sensor Microwave Imager (SSM/I; *F-8, -10, -11, -12, -13, -14,* and *-15*) and the Special Sensor Microwave Imager/Sounder (SSMIS; *F-16, -17,* and *18*)] was used to complement the geostationary IR imagery and examine the storm structure below the cirrus canopy for two TC cases in this study (Hawkins and Velden 2011; Hawkins et al. 2001; Lee et al. 2002). For the ice scattering channels (85, 89, and 91 GHz), the emissivity of water is low, making the ocean surface appear relatively cold, while the TC cirrus canopy is largely transparent. Additionally, scattering by larger snow and ice particles below the cirrus canopy and above the freezing level is more prevalent, making the satellite field of view appear colder. Therefore, this channel is ideal for examining TC inner-core and rainband structures in the middle to upper levels. The 37-GHz channel can detect emissions from below cirrus canopy, but is much less sensitive to precipitation-sized ice particles and more sensitive to low-level rain and cloud liquid water. Thus, this channel has utility for detecting lower to midlevel features in the storm environment. Together, the 85- and 37-GHz channels elucidate important details regarding the nature of the TC diurnal cycle detected in the geostationary IR imagery and provide information as to the approximate depth of the observed diurnal pulses.

Extended best track data (Demuth et al. 2006) was used to examine diurnal tendencies in the radii of 34-, 50-, and 64-kt ($1\,kt = 0.5144\,m\,s^{-1}$) winds for all TC cases in the 10-yr dataset. Additionally, output from the University of Wisconsin–Cooperative Institute for Meteorological Satellite Studies (CIMSS) advanced Dvorak technique (ADT; Olander and Velden 2007) was used to assess possible linkages between the TC diurnal cycle and satellite-based objective Dvorak intensity estimates.

Since the main objective of this effort is to identify diurnal variability in the TC and its surrounding environment, it was necessary to adjust the dataset into a LST framework. It is hypothesized that radiative responses at the cirrus canopy level near the time of sunset may be a critical driving mechanism for the TC diurnal cycle (discussed in section 4). This would suggest that the time of local sunset governs the evolution of the TC diurnal cycle processes described here. Since this time can vary by ~3 h across the North Atlantic basin from 1 June to 30 November, azimuthal calculations of IR brightness temperatures and 6-h IR brightness temperature trends performed relative to local sunset are probably the most robust way to represent the TC diurnal cycle. However, because LST provides a more familiar baseline to many readers, mean statistics relative to both LST and hours after sunset are presented.

## 3. Results

### a. 2007 Hurricane Felix

Figure 1 shows an example of the TC diurnal cycle for 2007 Hurricane Felix on 3 September while it was weakening from a category 5 with an intensity of $72\,m\,s^{-1}$ to a category 4 at $59\,m\,s^{-1}$. The GOES IR imagery suggests a rapidly expanding cirrus canopy in all quadrants between 1215 and 1815 UTC and asymmetries were

[2] This value falls within the 7–8 $m\,s^{-1}$ "critical shear" range for weakening versus strengthening North Atlantic TCs (Gallina and Velden 2000) and is slightly less than the mean 200–850-hPa vertical wind shear of the North Atlantic moist tropical sounding ($8.2\,m\,s^{-1}$; Dunion 2011).

[3] This criterion was applied for the landmasses of North America, including Cuba and Hispaniola. Smaller islands in the region were not considered to be land.

TABLE 1. 2001–10 North Atlantic major hurricane cases utilized in this study. The position, intensity, and vertical wind shear represent mean values over the period that were examined. The mean TC diurnal cycle (TCDC) trough-to-peak amplitudes ($R = 300$ km) calculated from the 6-h geostationary IR brightness temperature differencing imagery is also shown for each storm.

| Storm | Year | Dates | Lat (°N) | Lon (°W) | Intensity ($m\,s^{-1}$) | Shear ($m\,s^{-1}$) | TCDC amplitude (°C) $R = 300$ km |
|---|---|---|---|---|---|---|---|
| Erin | 2001 | 9–11 Sep | 33.4 | 63.2 | 49 | 6.1 | 21.5 |
| Felix | 2001 | 13–15 Sep | 28.7 | 45.3 | 46 | 5.9 | 30.3 |
| Iris | 2001 | 8 Oct | 17.1 | 83.9 | 54 | 4.9 | 39.4 |
| Michelle | 2001 | 3 Nov | 18.9 | 84.2 | 54 | 4.7 | 28.4 |
| Lili | 2002 | 1–2 Oct | 23.1 | 85.7 | 49 | 3.9 | 47.2 |
| Fabian | 2003 | 31 Aug–3 Sep | 19.0 | 56.2 | 61 | 6.4 | 33.0 |
| Isabel | 2003 | 12–15 Sep | 22.6 | 61.5 | 70 | 3.7 | 42.9 |
| Kate | 2003 | 3–4 Oct | 29.3 | 48.7 | 48 | 4.7 | 17.9 |
| Frances | 2004 | 31 Aug–2 Sep | 20.4 | 63.7 | 60 | 4.5 | 41.8 |
| Ivan | 2004 | 9–12 Sep | 16.2 | 74.6 | 68 | 5.2 | 30.0 |
| Jeanne | 2004 | 23–25 Sep | 26.2 | 72.0 | 43 | 5.7 | 34.3 |
| Karl | 2004 | 20–22 Sep | 20.3 | 47.1 | 57 | 5.6 | 26.0 |
| Dennis | 2005 | 9–10 Jul | 26.1 | 84.9 | 54 | 5.4 | 19.8 |
| Emily | 2005 | 15–17 Jul | 16.3 | 76.6 | 60 | 7.6 | 47.4 |
| Katrina | 2005 | 27–29 Aug | 26.0 | 87.6 | 65 | 4.6 | 34.8 |
| Maria | 2005 | 5 Sep | 31.6 | 56.7 | 44 | 7.7 | 23.7 |
| Rita | 2005 | 21–23 Sep | 25.2 | 88.1 | 72 | 4.9 | 24.7 |
| Wilma | 2005 | 19–20 Oct | 17.4 | 83.0 | 74 | 4.3 | 26.9 |
| Gordon | 2006 | 13–14 Sep | 26.2 | 57.6 | 45 | 6.4 | 41.9 |
| Helene | 2006 | 18–20 Sep | 23.8 | 51.7 | 49 | 4.3 | 21.5 |
| Dean | 2007 | 18–21 Aug | 16.8 | 75.4 | 69 | 3.7 | 34.7 |
| Felix | 2007 | 2–4 Sep | 12.9 | 69.2 | 56 | 3.5 | 64.9 |
| Bertha | 2008 | 7–10 Jul | 22.3 | 54.7 | 45 | 6.5 | 27.0 |
| Gustav | 2008 | 29 Aug–1 Sep | 21.4 | 79.1 | 48 | 6.4 | 33.1 |
| Ike | 2008 | 4–7 Sep | 22.0 | 58.4 | 59 | 5.7 | 15.2 |
| Paloma | 2008 | 7–8 Nov | 18.3 | 81.3 | 43 | 6.4 | 22.1 |
| Bill | 2009 | 18–21 Aug | 19.4 | 56.1 | 53 | 4.2 | 15.8 |
| Fred | 2009 | 9–10 Sep | 14.4 | 32.7 | 47 | 3.7 | 15.5 |
| Danielle | 2010 | 26–28 Aug | 26.3 | 58.2 | 50 | 4.5 | 32.0 |
| Earl | 2010 | 26–28 Aug | 19.5 | 64.7 | 56 | 4.2 | 39.6 |
| Julia | 2010 | 15 Sep | 17.2 | 31.5 | 49 | 5.9 | 12.4 |

clearly evident in the IR cloud field from $R = 100$ to 300 km during this time. These asymmetries were mainly associated with a large area of cold cloud tops (from −50° to −70°C) in the western and northern semicircles of the storm that appeared to be separating from the inner-core region during the morning hours (Fig. 1, top left; $R$ = ~150 km). By the early afternoon local time (Fig. 1, top right), this arc of cold cloud tops had propagated to a radius of ~250–350 km and an expanding gap of relatively warmer cloud tops (approximately from −30° to −40°C) evident between this feature and the storm's inner core.

Figure 1 also shows IR differencing imagery that depicts 6-h changes in the storm's IR temperature field from 0615 to 1215 UTC. The imagery indicates a circular ring (i.e., the diurnal pulse; yellow to pink shading) in the cloud field at approximately $R$ = 150–250 km that had cooled as much as 20°–50°C during this 6-h period, with areas of warming (cyan to blue shading, 5°–30°C) evident behind the diurnal pulse in the inner ~150 km. By 1815 UTC that day (Fig. 1, bottom-right panel), the diurnal pulse had propagated to a radius of ~250–350 km from the center and a broad circular area of warming inner core cloud tops (5°–40°C) was located on its inner edge at $R$ = ~(50–200) km. The arc-like feature of radially propagating cold cloud tops previously noted in the IR satellite imagery was also coincident with the position of the diurnal pulse in the IR differencing imagery. This suggests that it was, in fact, linked to the diurnal pulse seen propagating away from the storm that day. Although the diurnal pulse evolution is somewhat evident in the GOES IR images (Fig. 1, top panels), details and subtleties of its structure and position are better elucidated in the GOES IR differencing images (Fig. 1, bottom panels).

The 37- and 89–91-GHz microwave satellite images (from the NASA *Aqua* and DMSP satellites) shown in Fig. 2 are within ~1.5 h of the image times shown in Fig. 1 and confirm that the arc of cold cloud tops (i.e.,

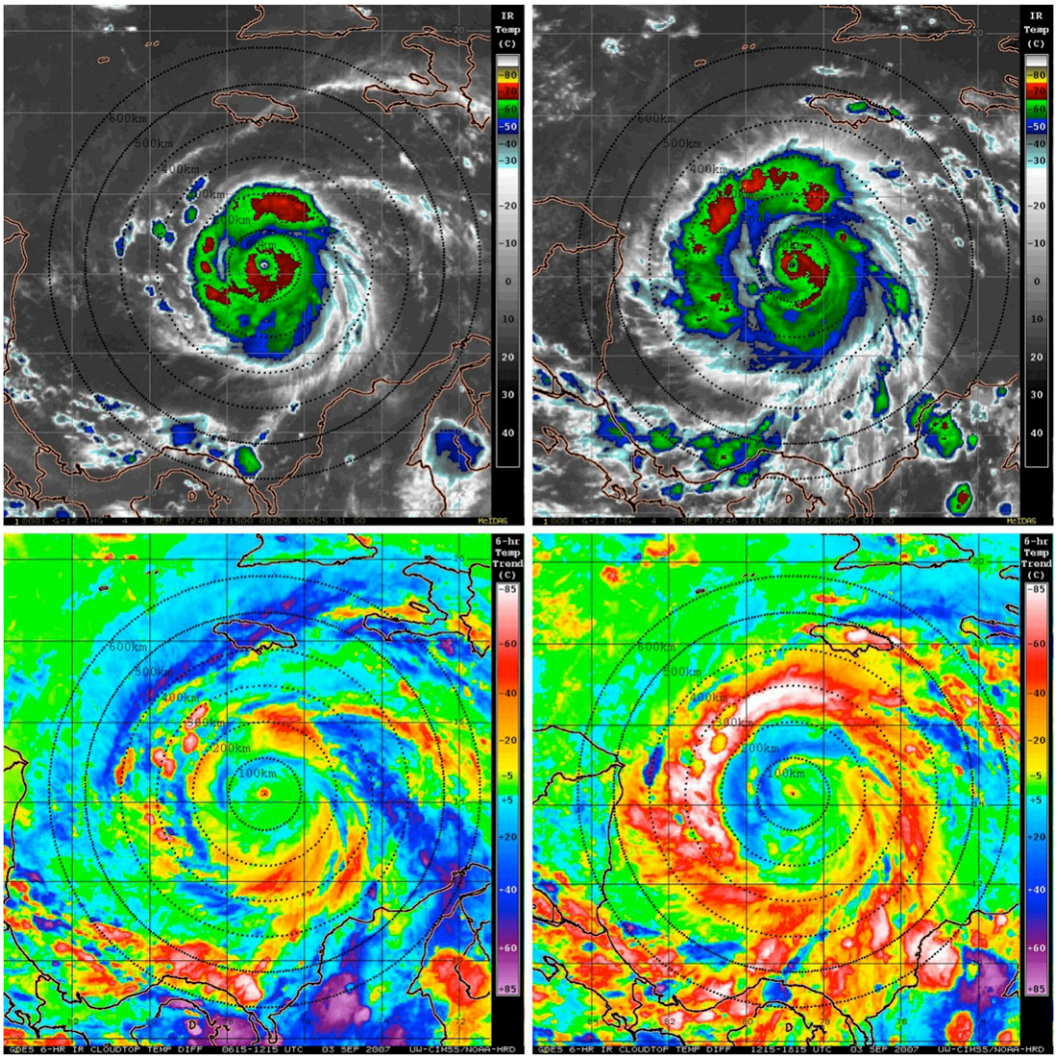


FIG. 1. (top) GOES IR imagery showing 2007 Hurricane Felix valid at (left) 1215 UTC (0715 LST) and (right) 1815 UTC (1315 LST) 3 Sep. (bottom) The corresponding 6-h GOES IR brightness temperature differencing images for these times . The yellow to pink shading (−10° to −85°C IR cooling tendencies) indicates a diurnal pulse propagating away from the storm during this period. The 100–600-km range rings (black dashed curves) from the TC center are overlaid on each of the satellite images. Lines of latitude and longitude are marked at 2° intervals.

diurnal pulse) in the western and northern semicircles of Felix was associated with outwardly expanding deep convection and was not just a shallow layer of cirrus outflow. The leading edge of this feature was denoted by cyan to pink shading (37 GHz) and brightness temperatures ranging from 175 to 250 K (89 and 91 GHz) in the microwave imagery and was positioned ~(175–200) km from the storm center at 1348 UTC (Fig. 2, left panels). By 1829 UTC, it was located at radii ranging from ~200 to 300 km (Fig. 2, right panels). Additional microwave satellite overpasses from NASA Tropical Rainfall Measuring Mission (TRMM) and other DMSP satellites confirmed this radial expansion (not shown). This is a significant observation and suggests that the TC diurnal cycle may be manifested in a deep layer of the TC environment and, therefore, may be an important influence on TC structure and possibly even intensity.

The outwardly propagating diurnal pulse and marked warming of the cloud tops at radii inside of the pulse appear to be key elements of the TC diurnal cycle and suggest that it has a radially dispersive nature. The structure of this propagating feature also suggests that minima and maxima associated with the TC diurnal cycle (e.g., cirrus canopy areal coverage, convection, and precipitation) cannot be adequately described in terms of time alone. Instead, the TC diurnal cycle is better described in terms of both time and space. To effectively capture this diurnal signal, azimuthal calculations of IR

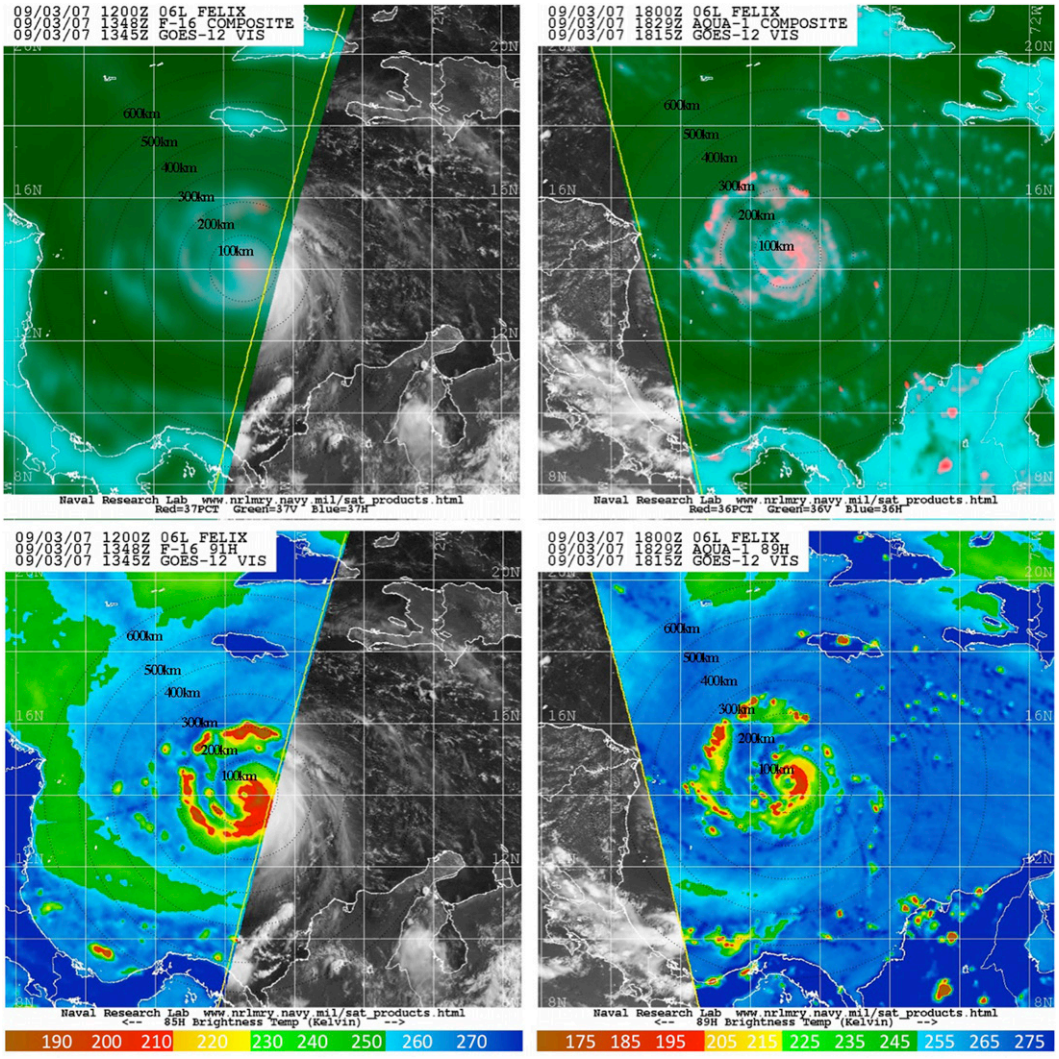


FIG. 2. (top) DMSP *F-16* SSMIS sensor and NASA *Aqua* AMSR-E 37-GHz color composite microwave satellite imagery (created from the horizontal and vertical polarizations and polarization-corrected temperatures) for 2007 Hurricane Felix valid at (left) 1348 UTC (0848 LST) and (right) 1829 UTC (1329 LST) 3 Sep. (bottom) The corresponding 89–91-GHz microwave images for these times. Note that the microwave overpass times are within 90-min of the respective GOES images shown in Fig. 1 and that areas outside of the satellite swath were supplemented by GOES visible imagery. The 100–600-km range rings (black dashed curves) from the TC center are overlaid on each of the satellite images. Lines of latitude and longitude are marked at 2° intervals. (Images provided courtesy of the Naval Research Laboratory in Monterey, CA.)

brightness temperatures and IR brightness temperature trends were generated for Hurricane Felix every 3 h from 2045 LST 1 September to 0145 LST 4 September at 100–600-km radii from the storm center. It should be noted that the 200–850-hPa vertical shear was quite low (0.5–6 m s$^{-1}$) throughout this period and consistently below the maximum shear criteria (7.5 m s$^{-1}$) discussed in section 2.

Figure 3 (top panel) shows a time series of azimuthal mean IR brightness temperature (200-, 300-, 400-, and 500-km radii) for Felix from 1 to 4 September, while the bottom panel shows the identical time period, only for calculations of IR brightness temperature trends. The former azimuthal calculations focus on the magnitude of IR brightness temperature fluctuations at various radii, while the latter calculations focus on the time tendency of this signal. There is some indication that the time tendency variability provides a more robust (i.e., exhibits higher and more consistent amplitude) depiction of the TC diurnal cycle and will be discussed in further in section 3c. A clear maximum cooling in the $R$ = 200–500-km satellite IR field is evident in both plots ranging from the early morning to late afternoon (local time),

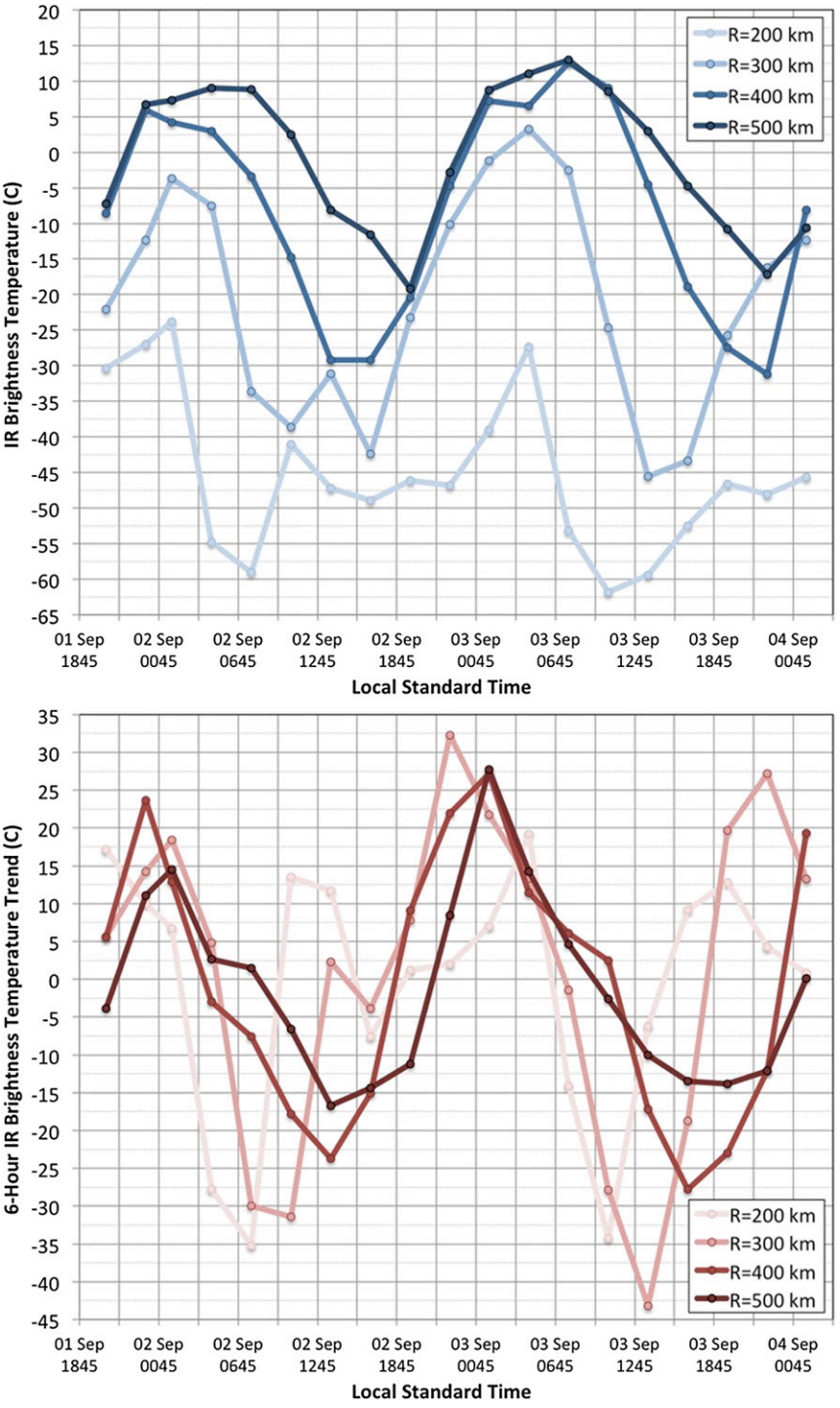


FIG. 3. Azimuthally averaged 3-hourly GOES (top) IR brightness temperatures and (bottom) 6-h brightness temperature trends at 200-, 300-, 400-, and 500-km radii around 2007 Hurricane Felix from 2045 LST 1 Sep to 0145 LST 4 Sep.

followed by a distinct maximum in warming from the early evening to early morning hours. The oscillatory nature of this cooling and warming is quite regular from day to day in these plots and suggests the repeatability of this phenomenon. Also of note is the apparent phase shift in the timing of the diurnal cycle at the various radii (i.e., the peak cooling–warming tended to progress radially outward in time from 200 to 500 km). These trends

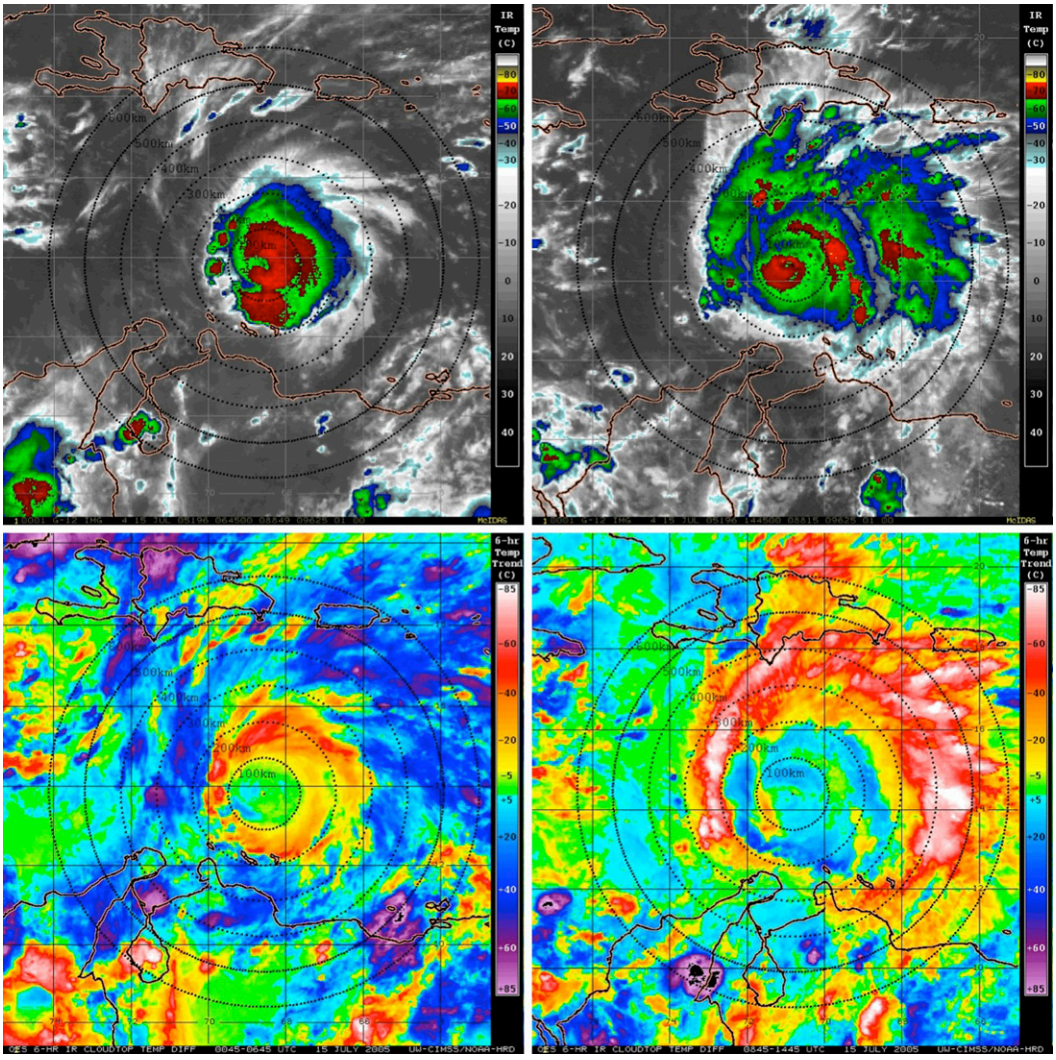


FIG. 4. As in Fig. 1, but for 2005 Hurricane Emily valid for (left) 0645 UTC (0145 LST) and (right) 1445 UTC (0945 LST) 15 Jul.

suggest that the TC diurnal cycle signal began at the innermost radii (e.g., <200 km, not shown) and propagated to peripheral radii at a speed of ~(5–10) m s$^{-1}$ during the course of several hours.

### b. 2005 Hurricane Emily

Figure 4 shows an example of the TC diurnal cycle for 2005 Hurricane Emily on 15 July. Emily was a powerful (category 4, 59 m s$^{-1}$), compact storm early that day (Fig. 4, top-left panel) and similar to the Felix case, exhibited rapid radial growth of its cirrus canopy throughout the late morning and afternoon (Fig. 4, top-right panel). Also similar to the Felix case, an arc of cold cloud tops was seen propagating away from Emily's inner core during this time. This diurnal pulse was especially evident in the western, northern, and eastern semicircles of the storm at ~$R$ = 150–350 km and a moat of warmer (−30° to −50°C) cloud tops was apparent on the inside edge of that pulse at ~$R$ = 150–250 km (Fig. 4, top-right panel).

Figure 4 (bottom-left panel) shows IR differencing imagery and depicts changes in Emily's IR temperature field from 0045 to 0645 UTC. As was seen in the Felix case, the imagery shows a remarkably circular ring feature at approximately $R$ = 100–250 km that had cooled 20°–60°C during this 6-h period, with warming of 5°–20°C evident on the inside edge of the diurnal pulse in the inner 100 km. By 1445 UTC that day the diurnal pulse had propagated to a radius of ~(250–400) km from the center and the inner-core cloud tops on its inside edge (0–200-km radius) had warmed by 5°–40°C (Fig. 4, bottom-right panel). The GOES IR images from those corresponding times (Fig. 4, top panels) reveal a storm

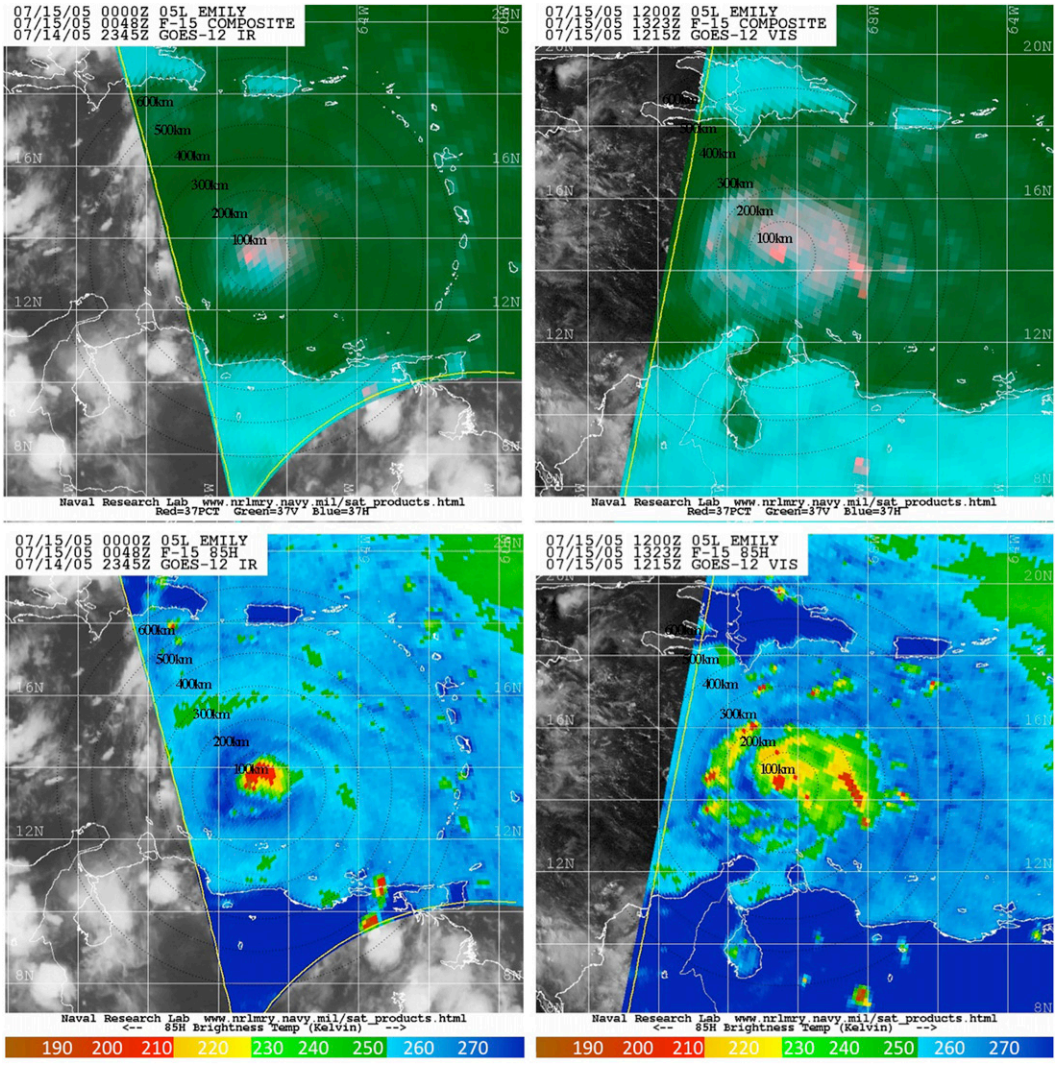


FIG. 5. As in Fig. 2, but for 2005 Hurricane Emily valid for (left) 0048 UTC (2048 LST) and (right) 1323 UTC (0823 LST) 15 Jul, with the DMSP *F-15* SSMIS sensor and with overpass times that are within ~6 and ~1.5 h of the respective GOES images shown in Fig. 4. (Images provided courtesy of the Naval Research Laboratory in Monterey, CA.)

with a much larger cirrus canopy and a structure that had visibly deteriorated (the NHC best track intensity for Emily dropped 10 m s$^{-1}$ during that afternoon). Similar to the Felix case, microwave satellite imagery (37 and 85 GHz) from the NASA *Aqua*, DMSP, and NASA TRMM satellites confirmed that the diurnal pulse that was seemingly propagating away from Emily's inner core in the GOES IR imagery was not just a cirrus outflow feature, but was instead a deep convective feature (Fig. 5). Figure 5 shows a significant radial expansion of the storm in the 37- and 85-GHz imagery (190–250-K brightness temperatures) from 0048 to 1323 UTC 15 July that was approximately collocated with the diurnal pulse signal shown in Fig. 4. In fact, the radial extent of the deep convection around the storm [i.e. cyan to pink shading (37 GHz) and ≤250-K brightness temperatures (85 GHz)] expanded by ~(125–200) km during that ~12.5-h period.

Figure 6 shows plots derived from azimuthal calculations of GOES IR brightness temperatures and 6-h IR brightness temperature trends for Hurricane Emily every 3 h from 2045 LST 14 July to 1845 LST 17 July at 200-, 300-, 400-, and 500-km radii from the storm center. Unlike the Felix case, the 200–850-hPa vertical wind shear for Emily reached values (9–11 m s$^{-1}$) above the 7.5 m s$^{-1}$ threshold described in section 2 for a portion of the storm's life cycle that was examined. This segment of Emily's life cycle was not included in the azimuthal mean statistics of the TC diurnal cycle presented in the next

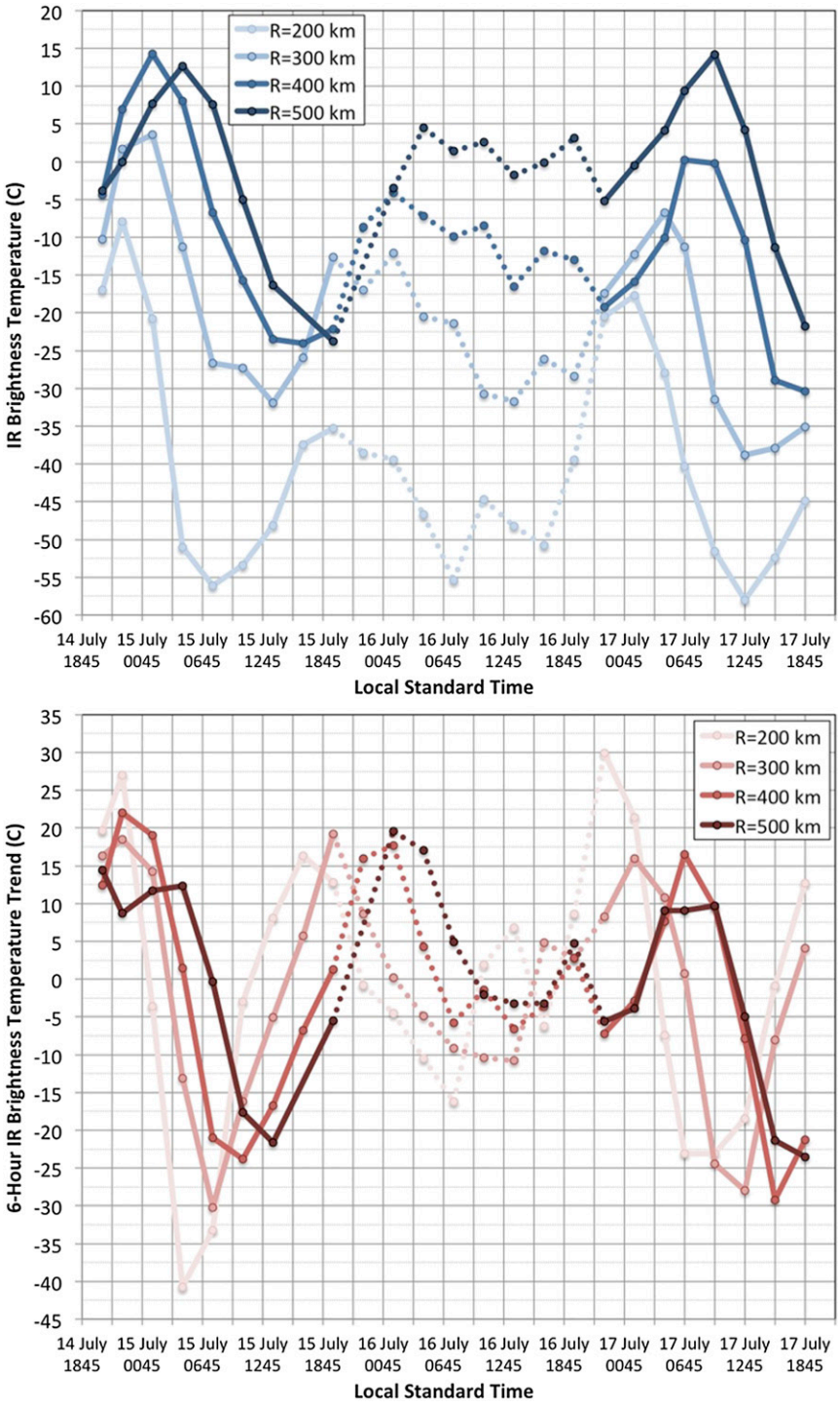


FIG. 6. Azimuthally averaged 3-hourly GOES (top) IR brightness temperatures and (bottom) 6-h brightness temperature trends at 200-, 300-, 400-, and 500-km radii around 2005 Hurricane Emily from 2045 LST 14 Jul to 1845 LST 17 Jul. The dashed curved lines represent periods when the 200–850-hPa vertical wind shear for Emily reached values (9–11 m $s^{-1}$) above the 7.5 m $s^{-1}$ threshold described in section 2.

section. The periods of lower shear ($\leq$7.5 m s$^{-1}$) at the beginning and end of the Emily time series show distinct diurnal cycle signals in the GOES IR brightness temperature fields, with peak cooling in the early morning to late afternoon hours (local time), followed by distinct maxima in warming during the early evening to early morning hours (Fig. 6, solid curves). Similar to the Felix case, the Emily analyses suggest that the radial propagation speed of the TC diurnal pulse signal was ~(5–10) m s$^{-1}$.

Relative to local time, the diurnal variations of warming and cooling in the Emily GOES IR brightness temperature field shown in Fig. 6 corresponded remarkably to those found in the Felix case (Fig. 3). This further suggests that the TC diurnal cycle has predictability in both time and space. Interestingly, the period of the Emily life cycle that exhibited moderate to high vertical wind shear (>7.5 m s$^{-1}$) was also marked by a diminished TC diurnal cycle signal (i.e., the brightness temperature magnitudes and time tendency amplitudes were reduced in the satellite IR fields during this time; Fig. 6, dashed curves). This could be related to weakening of inner-core processes that might be forcing the TC diurnal cycle and/or to the radial displacement of the cirrus canopy and deep convection in conditions of strong vertical wind shear. Asymmetries in the GOES IR brightness temperature field resulting from the latter process could lead to azimuthal calculations that do not adequately capture diurnal pulses that propagate away from the storm. Still, the TC diurnal cycle found in the Emily case exhibited notable similarity to that shown for the Felix case. These similarities suggest that a robust multistorm examination of the TC diurnal cycle could be carried out if the criteria discussed in section 2 are utilized and if the daily solar cycle is used to normalize the evolution of this phenomenon in time and space.

### c. *Diurnal pulse azimuthal analyses*

A spectral analysis of the entire 10-yr dataset of IR satellite imagery was performed to identify signals of the TC diurnal cycle at various radii from the storm center and confirm the cyclic nature of this phenomenon as suggested by the 2005 Hurricane Emily and 2007 Hurricane Felix cases. These analyses were carried out relative to LST on a detrended, concatenated time series created from all storms in the dataset and analyzed using an autoregressive [AR(1)] model. The spectral analyses were tested for significance against a Markov red noise continuum (Gilman et al. 1963). Figure 7 shows a spectral analysis of the IR brightness temperatures from $R$ = 100 to 600 km and corroborates some of the findings from Kossin (2002). A clear diurnal cycle (1 cycle per day) is evident in the IR brightness temperature field that appears to be more robust at peripheral radii (e.g., $\geq$200 km), yet is not as readily detectable at 100 km. Surprisingly, the semidiurnal (2.0 cycles per day) signal that was described by Kossin (2002) was not found at $R$ = 100 km in the current dataset. This suggests that if a semidiurnal cycle is indeed present in TCs at this inner radius, it may either not occur in major hurricanes or is just not readily detectable in the environments of these stronger storms. Figure 7 shows that even at the 200-km radius, the TC diurnal cycle signal is prominent, though it appears to be strongest at the 300- and 400-km radii. This suggests that the outwardly propagating diurnal pulse that has been discussed does not really become a distinct feature until $R$ = ~(150–200) km. It is not clear if this implies that the TC diurnal pulse tends to form in this intermediate radius range and is not typically found at the innermost radii or if the cyclonic circulation closer to the center is advecting cloud features around the storm and masking an otherwise active diurnal pulse signal in the spectra.

The diurnal cycle power spectrum shown in Fig. 7 also indicates that although the peak signal occurs at 300–400 km, this phenomenon is a prominent feature even at large radii (e.g., 500–600 km), far removed from the convective TC inner-core region. It is hypothesized that smaller-sized storms would tend to produce a less detectable diurnal pulse signal at 500–600 km. In fact, each storm may have a preferred radius where the power spectrum peaks and would be dependent on the size of the convectively active inner-core region. This is beyond the scope of the current study, but warrants further investigation.

Based upon the diurnal signal indicated in the spectral analysis of the 2001–10 dataset, azimuthal mean 6-h IR brightness temperature trends were calculated at the 400-km radius for a subset (12 storms) of the 31 North Atlantic major hurricanes examined in this study (Fig. 8).[4] Each time series represent continuous 72-h snapshots for each storm and were examined relative to both LST and hours after sunset in order to optimally capture this diurnal signal. Figure 8 shows that a well-defined TC diurnal cycle with very clear and predictable oscillations in the satellite IR brightness temperature fields emerges, even when numerous TCs are examined. The TC diurnal pulses (i.e., peak cooling in the IR field) typically reached the 400-km radius at ~(1100–1700) LST [~(17–23) h after sunset] and were straddled by periods of peak warming from ~2200 to 0500 LST [~(3–10) h after sunset].

[4] These cases contained the most complete and continuous 72-h life cycles in the 10-yr dataset and were therefore chosen to illustrate the cyclic nature of the TC diurnal cycle. However, they are also representative of the larger storm sample.

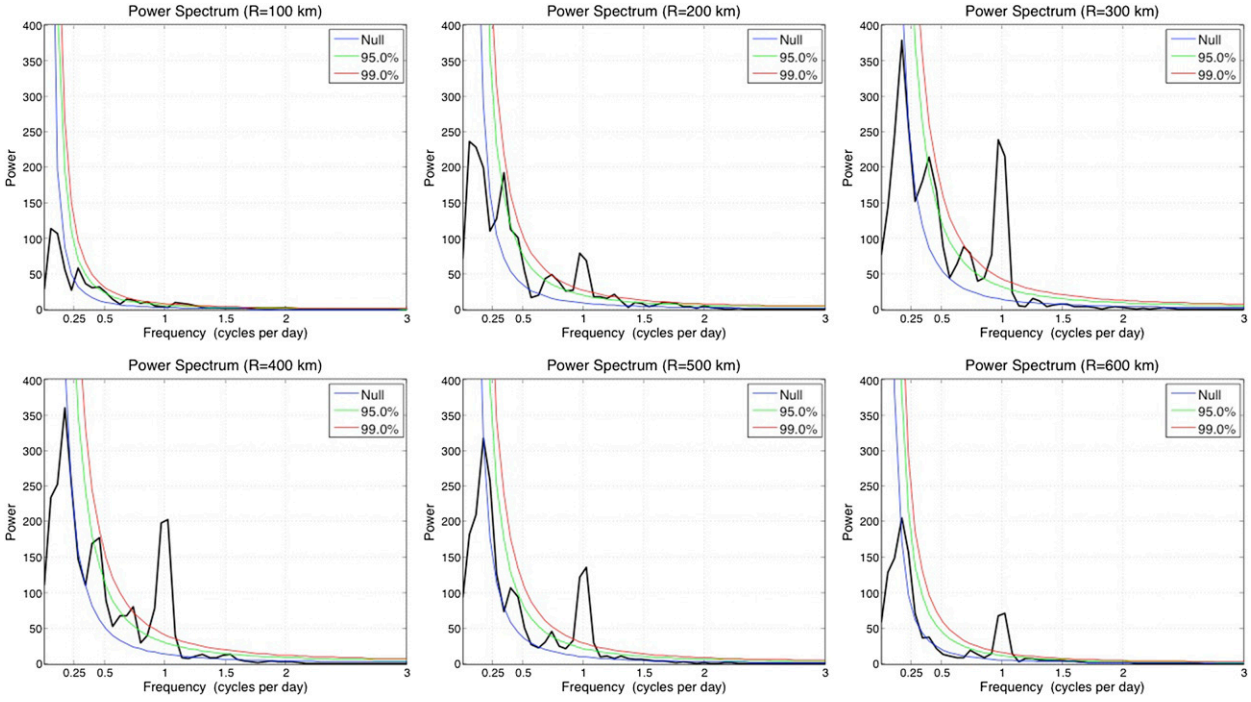


FIG. 7. Power spectrum of azimuthally averaged geostationary IR brightness temperatures for the 2001–10 North Atlantic major hurricanes that were investigated for $R = 100$–600 km. The colored curved lines indicated various confidence levels in the analyses (i.e., power values at or above these curves are statistically significant at the respective confidence levels).

Given the robustness of the TC diurnal signal depicted in Figs. 7 and 8, mean statistics were then calculated from 31 major Atlantic hurricanes from 2001 to 2010 using the selection criteria described in section 2. Figure 9 shows the mean azimuthal IR brightness temperatures and IR brightness temperature trends for these TCs every 3 h at 100–600-km radii from the storm center relative to LST. The IR brightness temperature trends at the 200–600-km radii (Fig. 9) point to a clear TC diurnal signal that is most pronounced (largest amplitudes) at the 300–400-km radii and is supported by the power spectrum analyses shown in Fig. 7. The TC diurnal cycle was not clearly evident at $R = 100$ km, similar to results shown in Fig. 7, as well as findings by Kossin (2002).

Several key conclusions can be drawn from the trends of geostationary 6-h IR brightness temperature trends shown in Fig. 9 regarding the nature of the TC diurnal cycle and its evolution in time and space. As previously mentioned, these 6-h IR brightness temperature trend plots more effectively captured the TC diurnal cycle. This figure also confirms the notion that the TC diurnal cycle and associated diurnal pulses propagate radially outward over time. Table 2 summarizes the diurnal pulse evolution relative to both LST and hours after local sunset and specifies the approximate timing of the passage of the TC diurnal pulse (and warming that precedes–follows it) at various TC radii. Figure 10 provides an alternative graphical representation of the mean TC diurnal pulse evolution over time and space. The diurnal pulses reach the 200-km radius (peak cooling in the IR field) at ~(0400–0800) LST [~(9–13) h after sunset], followed by the 300-km radius at ~(0800–1200) LST (13–17 h after local sunset), and the 400-km radius at ~(1200–1500) LST (17–20 h after local sunset). This implies a diurnal pulse propagation speed of 5–10 m s$^{-1}$. Each diurnal pulse also appears to be bounded by equally strong peaks in warming that occur ~(8–15) h before and after the passage of the diurnal pulse.

The oscillating peaks of cooling and warming evident in the IR satellite imagery may have important implications for the timing of TC inner-core convection (and possibly intensity change and precipitation). For instance, the diurnal pulse reaches $R = 200$ km at ~(0400–0800) LST [~(9–13) h after local sunset] and maximum warming (i.e., minimum in deep convection) occurs at ~(2000–0000) LST (1–5 h after local sunset). This corresponds well with Gray and Jacobson's (1977) findings regarding the timing of deep convection minima and maxima over tropical oceanic regions. However, the diurnal pulses pass through outer radii (e.g., 300–500 km) several hours after reaching $R = 200$ km (Fig. 9 and Table 2). This suggests that Gray and Jacobson's (1977)

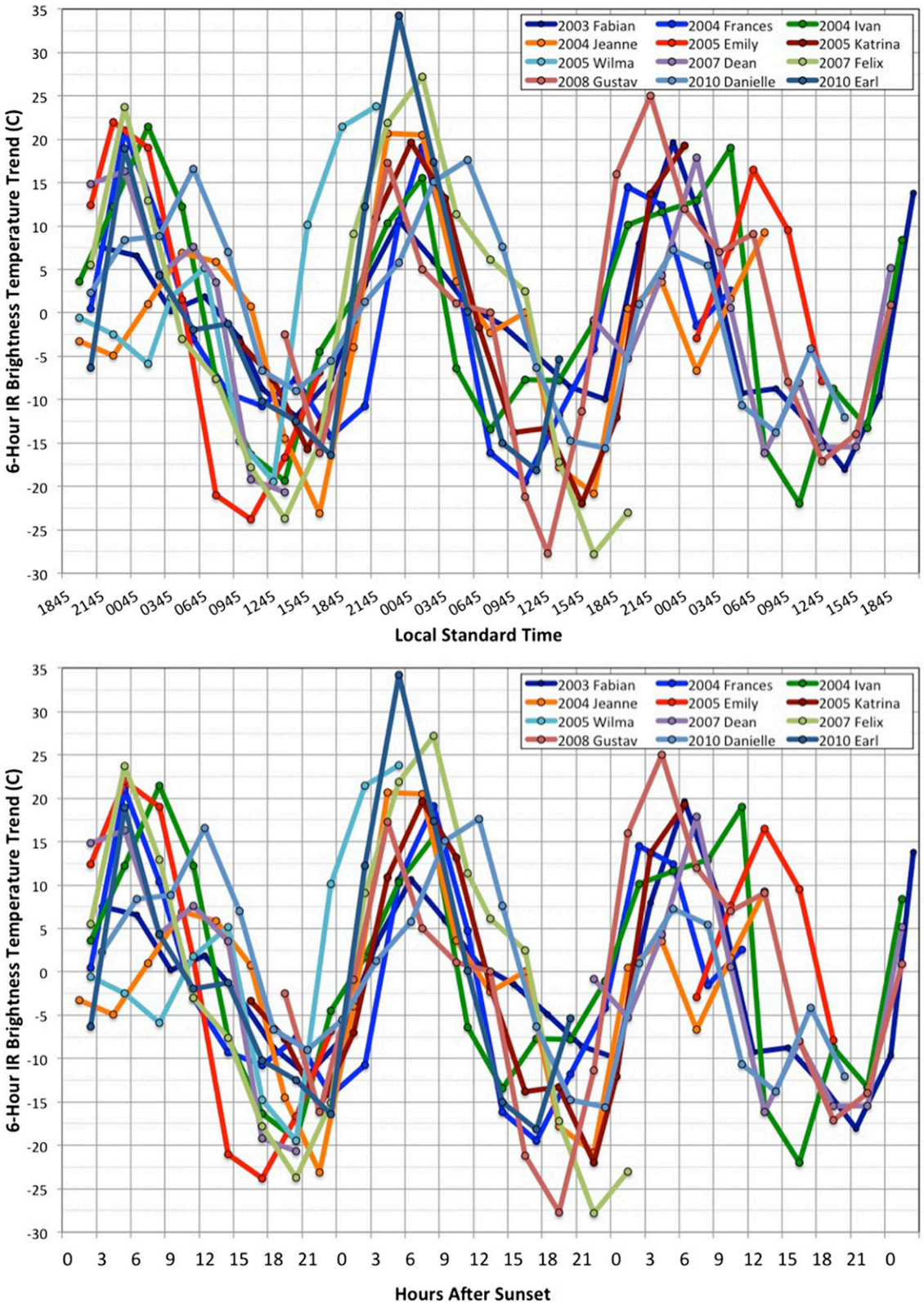


FIG. 8. Azimuthally averaged 3-hourly geostationary IR 6-h brightness temperature trends for several North Atlantic major hurricanes at a 400-km radius relative to (top) local standard time and (bottom) hours after local sunset.

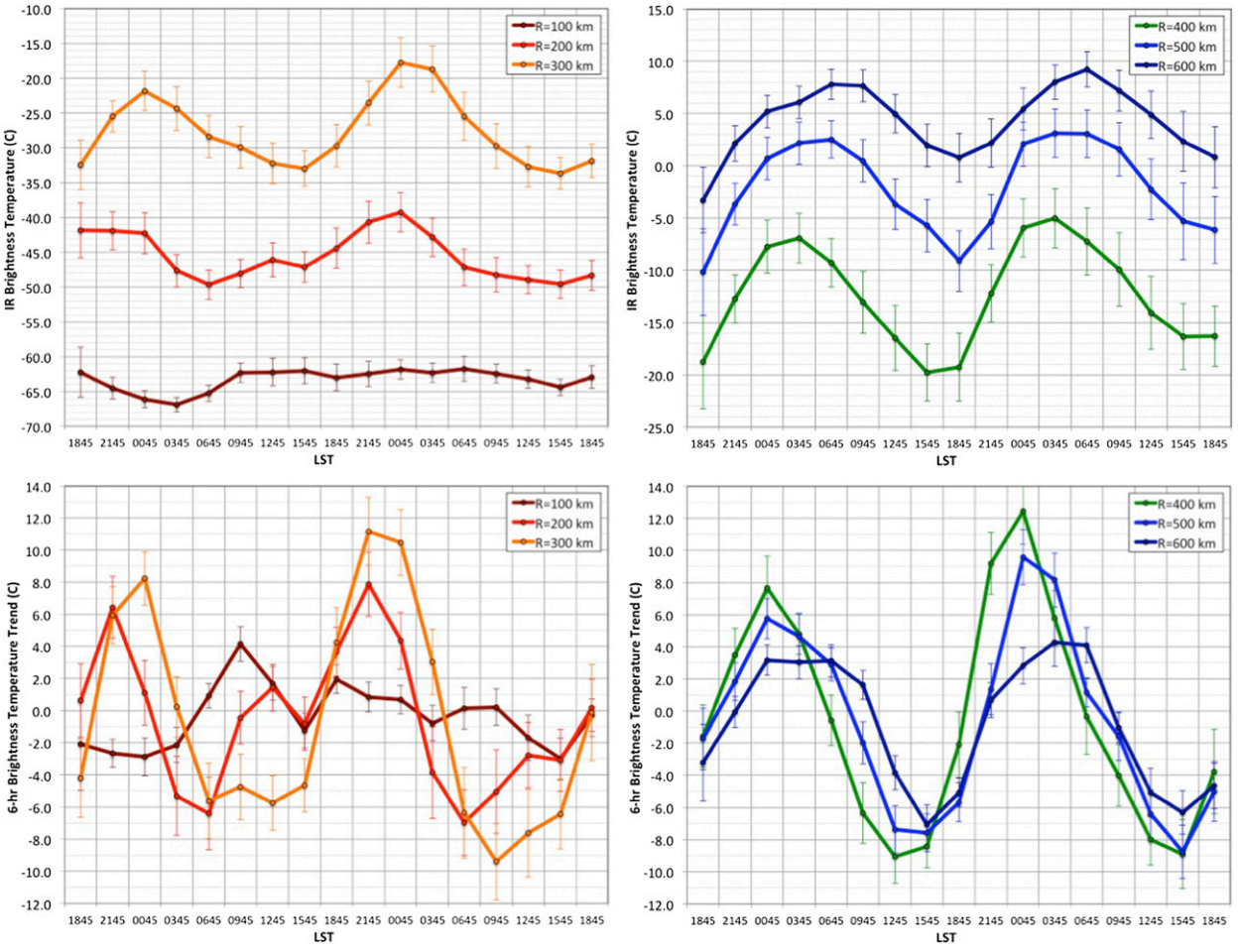


FIG. 9. (top) Azimuthally averaged 3-hourly geostationary IR brightness temperatures and standard error bars for the (left) 100–300-km radii and (right) 400–600-km radii relative to local standard time for all 31 North Atlantic major hurricanes that were examined. (bottom) The corresponding azimuthally averaged 6-h geostationary IR brightness temperature trends.

conclusions, although valid for the TC inner-core region, do not adequately describe the TC diurnal cycle at all radii for a storm. This relates to the fact that TC diurnal pulses propagate away from the TC center and hence, TC convective minima and maxima can be better described in terms of both time and space. Browner et al.'s (1977) findings regarding the minimum (0300 LST) and maximum (1700 LST) extent of the TC cirrus canopy also agree with the results shown in Fig. 9 and Table 2. However, it should be emphasized that the current work also puts these minima and maxima into a spatial context. Instead of a cirrus canopy with a single minimum and maximum extent, we propose that TC diurnal pulses may be propagating through a deep layer of the storm that includes the cirrus canopy and lower to middle troposphere.

TABLE 2. Mean timing of peak cooling and warming at the 200–600-km radii for the 2001–10 North Atlantic TC dataset relative to local standard time and the number of hours after sunset. The peak cooling represents the approximate timing of the TC diurnal pulse passage at a given radius.

| | $R$ = 200 km | $R$ = 300 km | $R$ = 400 km | $R$ = 500 km | $R$ = 600 km |
|---|---|---|---|---|---|
| Peak IR cooling | | | | | |
| LST | 0400–0800 | 0800–1200 | 1200–1500 | 1500–1800 | 1600–2000 |
| Hours after sunset | 9–13 | 13–17 | 17–20 | 20–23 | 21–25 |
| Peak IR warming | | | | | |
| LST | 2000–0000 | 2200–0200 | 2300–0300 | 0000–0400 | 0200–0600 |
| Hours after sunset | 1–5 | 3–7 | 4–8 | 5–9 | 7–11 |

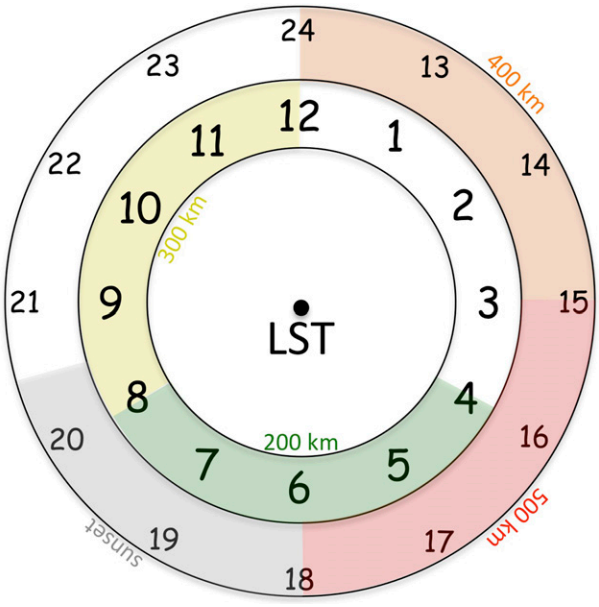


FIG. 10. A 24-h conceptual clock of the TC diurnal cycle evolution. Times listed are local standard time (LST) and colored shading denotes the approximate arrival time of the TC diurnal pulse at corresponding radii from the storm center. Arrival times are estimates and may vary depending on storm size.

### d. The TC diurnal cycle and TC structure

The results described in sections 3a–c show that the TC diurnal cycle impacts the thermal structure of the TC cirrus canopy and may impact TC structure through a relatively deep layer of the troposphere below the cirrus canopy. Since several earlier studies have also documented relationships between the areal extent and variance of satellite IR brightness temperature and the size of the TC wind field (Mueller et al. 2006; Kossin et al. 2007; Lee et al. 2010; Knaff et al. 2014), we examined the possible relationship between the TC diurnal cycle and TC structure using wind radii information from the extended best track dataset (Demuth et al. 2006). The entire 2001–10 dataset was used to examine diurnal fluctuations in the analyzed radii of 34-, 50-, and 64-kt 10-m surface winds with data binned into a single 3-hourly 24-h cycle for these analyses. It should be noted that the mean radii of 34-, 50-, and 64-kt winds for this limited sample of mature TCs was 230, 120, and 70 km, respectively. Table 3 shows an analysis of the radius of 50-kt winds derived from the extended best track and suggests that there are diurnal trends in the rate of expansion of the 50-kt wind radius around the storm depending on the time of day. The expansion of the 50-kt wind radius tends to reach a minimum in the early morning hours [~(0300–0900) LST] and peaks in the midafternoon to early evening hours [~(1800–2100) LST]. Though the trends for the 34 and 64 radii were similar to those of the 50-kt radii, the relationships were not as statistically significant. The weaker signals at these radii may relate to the fact that 34-kt radius is rarely sampled by reconnaissance aircraft and tends to be dominated by persistence from forecast cycle to forecast cycle, while the small mean radius of 64-kt winds (70 km) is in a region of the storm where the TC diurnal cycle signal is not readily detectable (see section 3c discussion). The diurnal fluctuations described here suggest that the surface wind fields of TCs may be influenced by the TC diurnal cycle and will be a focus of future study.

### e. The TC diurnal cycle and TC satellite intensity estimates

The ADT dataset was used to assess possible linkages between the TC diurnal cycle and satellite-based estimates of TC intensity. ADT represents an objective, automated version of the operational Dvorak technique for estimating TC intensity (Olander and Velden 2007). The algorithm utilizes ~11-$\mu$m IR imagery from geostationary satellites to examine various kinematic and thermodynamic properties of the TC cloud pattern. One of the output values from the ADT includes the raw tropical "*T*" number and the current intensity (CI) number (with a value range of 1.0–8.0). The former intensity estimate is determined from the analyzed Dvorak scene type (e.g., eye, central dense overcast, embedded center, curved band, and shear) and measured environmental parameters (e.g., scene temperatures and symmetry in the eye and cloudy regions of the storm) and has a final value that is not constrained in any way. The latter value is derived from the initial raw *T* number, but also includes operational rules and constraints that define how much a *T* number can change over a specified time interval. The CI number is empirically converted to an equivalent maximum sustained surface wind and a wind–pressure relationship is then used to assign the corresponding minimum sea level pressure (Velden et al. 2006). ADT TC intensity estimates are largely based upon pattern recognition of the IR satellite brightness temperature field and IR temperatures in the eye and surrounding cloud regions of the storm. Therefore, it is hypothesized that the TC diurnal cycle may also directly influence ADT satellite intensity estimates that are routinely used to determine TC intensity in ocean basins around the world. If this is the case, a spectral analysis of TC ADT estimates should show the existence of a diurnal signal within that dataset. Therefore, spectral analyses were performed on both the *T* numbers and CI numbers associated with each time series in the 2001–10 TC dataset using the criteria described in section 3c. Figure 11 indicates that a statistically significant (99% confidence level) diurnal cycle

TABLE 3. Diurnal trends (6 h) of 50-kt wind radii (R50) obtained from the extended best track for the entire 2001–10 dataset. Trough (0900 LST) to peak (1800 LST) trends in R50 were significant at the 99.9% level, determined using a two-tailed Student's *t* test. Time is in LST.

| R50 6-h trend (km) | 0000 | 0300 | 0600 | 0900 | 1200 | 1500 | 1800 | 2100 |
|---|---|---|---|---|---|---|---|---|
| Mean | +6.0 | +4.3 | +4.2 | +3.9 | +5.2 | +6.6 | +9.3 | +7.0 |
| Standard error | 0.77 | 0.76 | 1.02 | 1.01 | 0.38 | 0.91 | 1.18 | 0.95 |

(1 cycle per day) does indeed exist in the Dvorak raw $T$ number intensity estimates.

Curiously, the Dvorak raw $T$ numbers also exhibit a statistically significant cycle that is on the order of 0.5–0.75 cycles per day. This subdiurnal signal was also evident (95%–99% confidence level) in the Fig. 7 IR brightness temperature spectral analyses at $R$ = 100–600 km and is especially detectable at $R$ = 100–400 km. Given that Dvorak analyses are focused on IR brightness temperature information in the inner-storm radii [$R$ = ~(25–125) km], perhaps it is not surprising that the ADT and 100–400-km IR analyses show similar pattern in their spectra. It is not clear what is causing the 0.5–0.75 cycles per day signal in the Dvorak raw $T$ number spectral analysis and is beyond the scope of this current study. Future work should include investigating this subdiurnal signal in the ADT data, as well as possible repeatability in other Dvorak technique datasets (e.g., those produced at operational forecast centers). Although the spectral analysis of the Dvorak CI number also shows a similar peak at both 1 and 0.5–0.75 cycles per day (95% confidence level), the signal is not as pronounced as that of the Dvorak raw $T$ numbers. We hypothesize that operational constraints placed on the CI number could act to reduce the natural variability in TC structure that is associated with the diurnal cycle. Therefore, the differences between the $T$ number and CI number spectra suggest that there could be intensity biases built into the Dvorak technique that warrant further investigation.

## 4. Discussion

The observational evidence from geostationary and polar-orbiting microwave satellites shown in section 3 suggests that the TC diurnal cycle manifests itself as a pulse in the cloud field each day that involves a deep layer of the storm extending from the cirrus canopy down to altitudes below the freezing level. Although this indicates that the TC diurnal cycle may have an important influence on TC structure and possibly intensity, the exact mechanism(s) forcing this phenomenon is (are) not clear. Several hypotheses have been previously presented that attempt to address the causes for observed fluctuations in atmospheric deep convection. We only briefly describe these hypotheses, recognizing that a more detailed analysis (e.g., using a combination of satellite data, in situ thermodynamic and kinematic measurements, and numerical model output) of each of them is required to assess their merit.

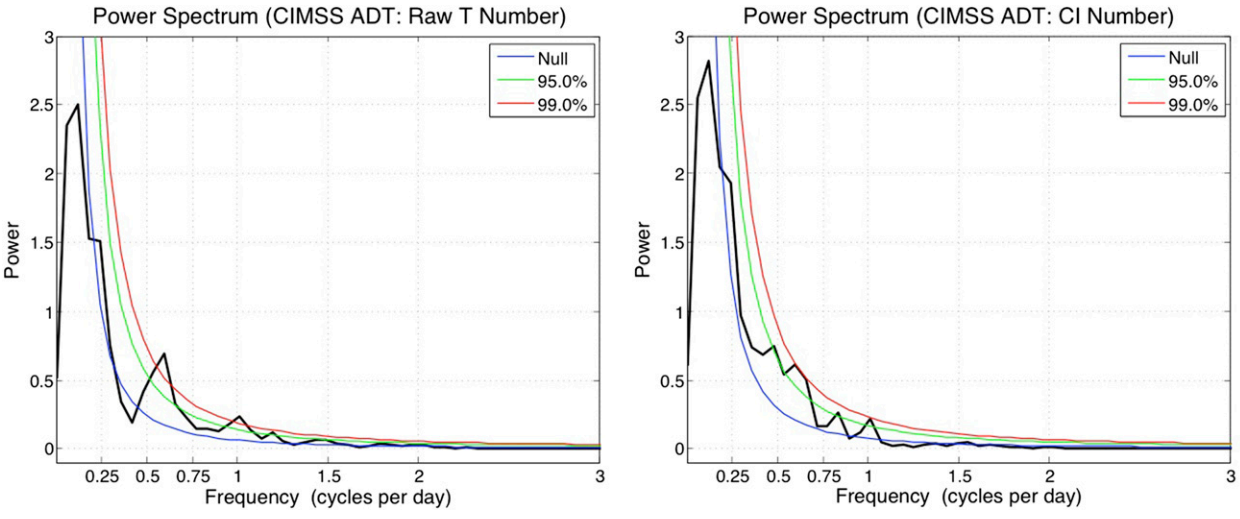


FIG. 11. Power spectrum of the advanced Dvorak technique (left) raw $T$ numbers and (right) CI numbers for the 2001–10 North Atlantic major hurricanes that were investigated. The colored curved lines indicate various confidence levels in the analyses (i.e., power values at or above these curves are statistically significant at the respective confidence levels).

### a. Convectively driven atmospheric gravity waves

The remarkable symmetry of many of the TC diurnal pulses that were observed in this study suggests that they may be a propagating gravity wave feature. During the day, convectively generated gravity waves are produced in the TC inner core and propagate upward into the stratosphere (e.g., Pfister et al. 1993), but would generally remain undetectable by conventional observations (e.g., satellite imagery). However, it is possible that rapid radiative cooling at the level of the TC cirrus canopy near the time of sunset in concert with vertical wind shear associated with the TC upper-level outflow layer could generate a more statically stable vertical profile that would be capable of reflecting these convectively generated gravity waves (Tripoli and Cotton 1989). During this time, these trapped gravity waves would likely intensify in the troposphere as they propagate away from the storm close to the level of the cirrus canopy and would become more readily detectable (e.g., via satellite imagery) as they move through this cloud layer. These ideas will need to be studied both observationally and theoretically.

### b. Radiatively reduced outflow resistance

Outflow resistance as measured by inertial available kinetic energy (IAKE) is tied intrinsically to the potential vorticity of the outflow layer (Mecikalski and Tripoli 1998) and is defined as

$$\text{IAKE} = \int_{r=0}^{\text{RNA}} \frac{dU_{\text{rad}}}{dt} dR, \qquad (1)$$

where $U_{\text{rad}}$ is the radial velocity relative to a given point (in cylindrical coordinates) and $R$ is the total distance from the cloud plume origin ($r = 0$) to the radius of neutral acceleration (RNA). The potential vorticity of the outflow layer, in turn, is tied to the static stability of that layer, which is modulated diurnally by solar forcing, particularly when filled with outflow cirrus. Convective bands, as well as the developing storm convective core are suppressed by outflow resistance, particularly in the early stages of a TC when the outflow layer has not been strongly modified by the storm's own outflow and so remains particularly resistant to the formation of new outflow. Longwave cooling, beginning just before sunset destabilizes this outflow layer, dramatically reduces the potential vorticity of the layer and increases the IAKE, perhaps making it actually positive. This would lead to the release of outflow, and a response to the convection below, previously limited by the outflow resistance. Measurements of the potential vorticity evolution in the outflow layer should be made to supply observational confirmation of this potentially advective effect.

### c. Cloud–cloud-free differential heating mechanism

Gray and Jacobson (1977) described the notion that the cirrus canopy radiationally cools more at night and less during the day than surrounding cloud-free regions. The resulting pressure surfaces created by these temperature contrasts promote enhanced upper-level divergence and low-level convergence during the nighttime and early morning hours and could conceivably promote a period of enhanced upper-level outflow that could force the outward-propagating TC diurnal pulses that have been observed moving away from the storm at night. This process would suggest the TC diurnal pulses are, in fact, advectively driven features. Although Liu and Moncrieff (1998) concluded that this type of process was a secondary influence controlling the convective diurnal cycle in their model simulations, the cloud clusters that they examined were either fast moving or developed randomly in their model domain. It is conceivable that cloud–cloud-free differential heating processes could be more important in a more organized, longer-lasting convective system such as a TC.

### d. Direct radiation–convection interactions

This hypothesis was discussed by Kraus (1963), Chen and Cotton (1988), and later by Randall et al. (1991) and offers the idea that during the day, solar warming of the convective region cirrus canopy reduces the local lapse rate and promotes increased static stability in the middle to upper troposphere. Conversely, at night, preferential cooling at the level of the cirrus canopy relative to the lower troposphere decreases the static stability. These diurnal radiative trends would act to enhance convection during the nighttime and early morning hours and could also enhance upper-level divergence during these times. It is plausible that in the TC peripheral environment (e.g., $R$ = 150–200 km), relatively shallow convective areas (e.g., spiral bands) could especially benefit from the reduced mid to upper-level static stability that direct radiation–convection interaction processes would promote. It is also possible that nighttime and early morning periods of enhanced upper-level divergence could promote the observed TC diurnal pulses by promoting outward radial advection.

### e. Seeder-feeder mechanism

Houze et al. (1981) hypothesized that the enhancement of precipitation in warm-frontal rainbands can result when ice particles from aloft fall into the layer below the −4°C level and aggregate just above the melting level. These ''seeder'' ice crystals can subsequently, as they descend, help convert cloud water to precipitation via Bergeron–Findeisen processes (Bergeron 1935). Houze

et al. (1981) also described a second mechanism by which enhanced mesoscale lifting can increase the amount of ''feeder'' cloud water by condensation of vapor at low levels. It is possible that ice crystals associated with a radially expanding cirrus canopy in a TC environment (initiated by one of the three processes described in sections 4a–d) could help stimulate convection in peripheral rainbands via the seeder mechanism. Additionally, mesoscale lift associated with a radially propagating gravity wave of sufficient depth could promote the feeder mechanism.

Although the exact nature of the TC diurnal cycle and associated diurnal pulse are uncertain, more than one of the above hypothesized mechanisms (or another mechanism not considered here) could be acting together in the TC environment to produce this diurnal phenomenon. This idea is supported by preliminary findings from this study suggesting that TC diurnal cycle pulses affect a significant depth of the TC. For example, radial expansion of the cirrus canopy initiated by one or more of the gravity wave or advective processes described above could act in concert with the seeder-feeder mechanism to create a diurnal pulse that extends from the lower troposphere up to the cirrus canopy level. While the observation of the TC diurnal cycle is easily tracked by satellite and readily predictable in time and space, the causalities are still not clear and require additional study. High-resolution numerical modeling analyses (e.g., Nolan et al. 2013; Aksoy 2013) could be used to examine each of the proposed TC diurnal cycle driving mechanisms in isolation, as well as the possibility that multiple mechanisms are acting in concert to generate this atmospheric phenomenon.

## 5. Conclusions

A satellite-based examination of the tropical cyclone (TC) diurnal cycle is presented that expands on previous studies and attempts to quantify this phenomenon in both time and space. The dataset that was used included storm-centered infrared (IR) and 6-h IR brightness temperature differencing imagery for continuous 72-h periods for all North Atlantic major hurricanes from 2001 to 2010. The IR differencing imagery revealed a distinct diurnal pulse in the investigated storms that begins each evening near the time of local sunset and appears as a radially expanding, quasi-symmetric ring of cooling brightness temperatures with marked warming on its inside edge. The diurnal pulse appears to steadily move/propagate outward, reaching peripheral radii of the storm by early afternoon local time the following day. The TC diurnal cycle and associated diurnal pulses were shown to be closely linked to the daily solar cycle and preliminary analyses of microwave imagery suggested that it may involve a deep layer of the troposphere [~(200–600) hPa] as it moves–propagates away from the storm each day. Potential links between the TC diurnal cycle and TC structure and intensity was also supported by analyses of extended best track and advanced Dvorak technique (ADT) datasets. Additionally, geostationary IR imagery was used to examine azimuthal-mean brightness temperatures associated with TC diurnal pulses and suggested that this feature is highly predictable in both time and space. Although the exact nature of the TC diurnal cycle and diurnal pulses is still unclear, it is hypothesized that the solar cycle is a driving mechanism. The mechanisms controlling its evolution each day are also unclear, though several hypotheses are presented. Several main conclusions can be made from this study and the 10-yr dataset used to examine the TC diurnal cycle:

- This study highlights a diurnal cycle pattern in mature tropical cyclones that can be described as a dynamic process that evolves in both time and space. A 24-h conceptual clock has been proposed that approximates its temporal and spatial evolution.
- The TC diurnal cycle appears to be associated with a pulse in the cloud field that begins near the time of local sunset as a cooling region of inner-core cloud tops in geostationary IR differencing satellite imagery. This region of cooling cloud tops subsequently takes on a ringlike appearance as marked cloud-top warming begins to occur on its inside edge and it begins to move–propagate away radially from the storm at 5–10 $m\,s^{-1}$. A spectral analysis of the raw IR satellite dataset shows that it exhibits a clear diurnal signal.
- The period from local sunset to around sunrise [~(0–12) h after local sunset] is the most optimal time of day for TC inner-core deep convection (i.e., relatively colder inner-core cloud tops are evident in the IR imagery). The TC diurnal pulse is typically located at $R = <200$ km from the storm center during this period.
- The period from local midmorning to late afternoon [~(15–23) h after local sunset] is the least optimal time of day for TC inner-core deep convection (i.e., relatively warmer inner-core cloud tops are evident in the IR imagery). The TC diurnal pulse is typically located at $R = 300$–600 km from the storm center during this time.
- Microwave satellite imagery suggests that TC diurnal pulses might not be confined to the TC outflow layer, but instead may involve a relatively deep layer [e.g., ~(200–600) hPa] of the storm from the upper troposphere to an area near the melting level.

- Diurnal variability in extended best track radii of 50-kt winds was detected and suggests that the TC diurnal cycle may influence TC structure.
- A spectral analysis of objective ADT data suggests that these satellite-based TC intensity estimates exhibited a statistically significant diurnal signal. A subdiurnal signal was also found in the ADT data. These results suggest that ADT (and possibly other operational subjective Dvorak technique) estimates of TC intensity may be impacted by the TC diurnal cycle and that these estimates may also be associated with predictable biases that are dependent on the local time of day.
- Sunset appears to be a critical time for the initiation of the TC diurnal cycle and associated diurnal pulses. One or more possible hypothesized mechanisms could be controlling the initiation and subsequent evolution of this phenomenon: convectively driven atmospheric gravity waves originating in the TC inner core, radiatively reduced outflow resistance, cloud–cloud-free differential heating, direct radiation–convection interactions, or seeder-feeder mechanisms.

This study presents evidence for an observable TC diurnal cycle that is predictable in both time and space that may have implications for TC structure and intensity change. Future work that examines the TC diurnal cycle will require detailed observational and modeling efforts in order to advance our understanding of this potentially fundamental atmospheric process. Investigations should include analyses of diurnal trends in radiation at the level of the TC cirrus canopy as well as the surrounding clear-air atmosphere, diurnal changes in static stability, and upper-level divergence in the TC inner-core region and particularly at peripheral radii (e.g., 100–200 km), the relationship between TC diurnal pulses and the environmental thermodynamics that these pulses move through, and alternative means of tracking them (e.g., testing the feasibility of both 3-hourly image differencing and the utility of satellite image differencing using water vapor channels). Also, this current work specifically describes the development and evolution of the tropical cyclone diurnal cycle over oceanic regions. Since the characteristics of the tropical oceanic diurnal cycle and the convective diurnal cycle over land are quite unique, further investigation is needed to describe how these differing cycles relate to deep convection. Specifically, it is unclear how they might impact convective features that are transitioning from either over land to oceanic regimes (e.g., African easterly waves) or from oceanic to overland regimes (e.g., landfalling TCs).

The repeatability of TC diurnal pulsing in time and space suggests that it may be an undiscovered, yet fundamental TC process. Future work will examine possible links between TC diurnal pulses and the occurrence of extensive (i.e., hundreds of kilometers in length) low-level arc clouds and upper-level transverse bands, as there is some indication that these features may preferentially form along the leading edge of TC diurnal pulses (not shown). Given the apparent radial expansion of the TC cloud field that appears to occur in well-developed storms through a deep layer of the troposphere during the TC diurnal cycle, investigation of the possible relationship between TC diurnal pulses and eyewall replacement cycles is also warranted. Preliminary findings (not shown) also suggest that the TC diurnal cycle may occur in TCs globally and might not be exclusive to mature TCs. There is some indication that a convective diurnal cycle also occurs with other types of organized convection in both the tropics and midlatitudes (e.g., African easterly waves and mesoscale convective systems). The capability to monitor the TC diurnal cycle is an important initial step toward trying to better understand its characteristics, evolution, and potential implications.

*Acknowledgments.* The authors thank Frank Marks, John Molinari, Ryan Torn, Lance Bosart, and Greg Tripoli for many insightful discussions related to the TC diurnal cycle. This paper benefited from reviews by Rob Rogers from the Hurricane Research Division, NOAA/Atlantic Oceanographic and Meteorological Laboratory; Altug Aksoy from the Cooperative Institute for Marine and Atmospheric Studies, University of Miami, and Hurricane Research Division, NOAA/Atlantic Oceanographic and Meteorological Laboratory; Jeff Hawkins from Naval Research Laboratory, Monterey, California; and John Knaff from NOAA/NESDIS.

## REFERENCES

Aksoy, A., 2013: Storm-relative observations in tropical cyclone data assimilation with an ensemble Kalman filter. *Mon. Wea. Rev.,* **141,** 506–522, doi:10.1175/MWR-D-12-00094.1.

Bergeron, T., 1935: On the physics of cloud and precipitation. *Proc. Fifth Assembly U.G.G.I. Lisbon,* Vol. 2, Lisbon, Portugal, UGGI, 156 pp.

Browner, S. P., W. L. Woodley, and C. G. Griffith, 1977: Diurnal oscillation of cloudiness associated with tropical storms. *Mon. Wea. Rev.,* **105,** 856–864, doi:10.1175/1520-0493(1977)105<0856:DOOTAO>2.0.CO;2.

Chen, S., and W. R. Cotton, 1988: The sensitivity of a simulated extratropical mesoscale convective system to longwave radiation and ice-phase microphysics. *J. Atmos. Sci.,* **45,** 3897–3910, doi:10.1175/1520-0469(1988)045<3897:TSOASE>2.0.CO;2.

DeMaria, M., M. Mainelli, L. K. Shay, J. A. Knaff, and J. Kaplan, 2005: Further improvement to the Statistical Hurricane Intensity Prediction Scheme (SHIPS). *Wea. Forecasting,* **20,** 531–543, doi:10.1175/WAF862.1.

Demuth, J., M. DeMaria, and J. A. Knaff, 2006: Improvement of advanced microwave sounder unit tropical cyclone intensity

and size estimation algorithms. *J. Appl. Meteor. Climatol.,* **45,** 1573–1581, doi:10.1175/JAM2429.1.

Dunion, J. P., 2011: Rewriting the climatology of the tropical North Atlantic and Caribbean Sea atmosphere. *J. Climate,* **24,** 893–908, doi:10.1175/2010JCLI3496.1.

Gallina, G. M., and C. S. Velden, 2000: A quantitative look at the relationship between environmental vertical wind shear and tropical cyclone intensity change utilizing enhanced satellite derived wind information. Preprints, *24th Conf. on Hurricanes and Tropical Meteorology,* Ft. Lauderdale, FL, Amer. Meteor. Soc., 7A.4. [Available online at https://ams.confex.com/ams/last2000/webprogram/24HURRICANES.html.]

Gilman, D. L., F. J. Fuglister, and J. M. Mitchell Jr., 1963: On the power spectrum of ''red noise.'' *J. Atmos. Sci.,* **20,** 182–184, doi:10.1175/1520-0469(1963)020<0182:OTPSON>2.0.CO;2.

Gray, W. M., and R. W. Jacobson, 1977: Diurnal variation of deep cumulus convection. *Mon. Wea. Rev.,* **105,** 1171–1188, doi:10.1175/1520-0493(1977)105<1171:DVODCC>2.0.CO;2.

Hawkins, J. D., and C. Velden, 2011: Supporting meteorological field experiment missions and post-mission analysis with satellite digital data and products. *Bull. Amer. Meteor. Soc.,* **92,** 1009–1022, doi:10.1175/2011BAMS3138.1.

——, T. F. Lee, K. Richardson, C. Sampson, F. J. Turk, and J. E. Kent, 2001: Satellite multisensor tropical cyclone structure monitoring. *Bull. Amer. Meteor. Soc.,* **82,** 567–578, doi:10.1175/1520-0477(2001)082<0567:RIDOSP>2.3.CO;2.

Houze, R. A., S. A. Rutledge, T. J. Matejka, and P. V. Hobbs, 1981: The mesoscale and microscale structure and organization of clouds and precipitation in midlatitude cyclones. III: Air motions and precipitation growth in a warm-frontal rainband. *J. Atmos. Sci.,* **38,** 639–649, doi:10.1175/1520-0469(1981)038<0639:TMAMSA>2.0.CO;2.

Jarvinen, B. R., C. J. Neumann, and M. A. S. Davis, 1984: A tropical cyclone data tape for the North Atlantic basin, 1886–1983: Contents, limitations, and uses. NOAA Tech. Memo. NWS NHC 22, 21 pp.

Knaff, J. A., S. P. Longmore, and D. A. Molenar, 2014: An objective satellite-based tropical cyclone size climatology. *J. Climate,* **27,** 455–476, doi:10.1175/JCLI-D-13-00096.1.

Kossin, J. P., 2002: Daily hurricane variability inferred from GOES infrared imagery. *Mon. Wea. Rev.,* **130,** 2260–2270, doi:10.1175/1520-0493(2002)130<2260:DHVIFG>2.0.CO;2.

——, J. A. Knaff, H. I. Berger, D. C. Herndon, T. A. Cram, C. S. Velden, R. J. Murnane, and J. D. Hawkins, 2007: Estimating hurricane wind structure in the absence of aircraft reconnaissance. *Wea. Forecasting,* **22,** 89–101, doi:10.1175/WAF985.1.

Kraus, E. B., 1963: The diurnal precipitation change over the sea. *J. Atmos. Sci.,* **20,** 551–556, doi:10.1175/1520-0469(1963)020<0551:TDPCOT>2.0.CO;2.

Lazzara, M. A., and Coauthors, 1999: The Man computer Interactive Data Access System: 25 Years of Interactive Processing. *Bull. Amer. Meteor. Soc.,* **80,** 271–284, doi:10.1175/1520-0477(1999)080<0271:TMCIDA>2.0.CO;2.

Lee, C. S., K. K. W. Cheung, W.-T. Fang, and R. L. Elsberry, 2010: Initial maintenance of tropical cyclone size in the western North Pacific. *Mon. Wea. Rev*., **138,** 3207–3223, doi:10.1175/2010MWR3023.1.

Lee, T. F., F. J. Turk, J. D. Hawkins, and K. A. Richardson, 2002: Interpretation of TRMM TMI images of tropical cyclones. *Earth Interact.,* **6,** doi:10.1175/1087-3562(2002)006<0001:IOTTIO>2.0.CO;2.

Liu, C., and M. W. Moncrieff, 1998: A numerical study of the diurnal cycle of tropical oceanic convection. *J. Atmos. Sci.,* **55,** 2329–2344, doi:10.1175/1520-0469(1998)055<2329:ANSOTD>2.0.CO;2.

Mapes, B. E., and R. A. Houze Jr., 1993: Cloud clusters and superclusters over the oceanic warm pool. *Mon. Wea. Rev.,* **121,** 1398–1415, doi:10.1175/1520-0493(1993)121<1398:CCASOT>2.0.CO;2.

Mecikalski, J. R., and G. J. Tripoli, 1998: Inertial available kinetic energy and the dynamics of tropical plume formation. *Mon. Wea. Rev.,* **126,** 2200–2216, doi:10.1175/1520-0493(1998)126<2200:IAKEAT>2.0.CO;2.

Mueller, K. J., M. DeMaria, J. A. Knaff, J. P. Kossin, and T. H. Vonder Haar, 2006: Objective estimation of tropical cyclone wind structure from infrared satellite data. *Wea. Forecasting,* **21,** 990–1005, doi:10.1175/WAF955.1.

Nolan, D. S., R. M. Atlas, K. T. Bhatia, and L. R. Bucci, 2013: Development and validation of a hurricane nature run using the joint OSSE nature run and WRF model. *J. Adv. Model. Earth Syst.,* **5,** 382–405, doi:10.1002/jame.20031.

Olander, T. L., and C. S. Velden, 2007: The Advanced Dvorak Technique: Continued development of an objective scheme to estimate tropical cyclone intensity using geostationary infrared satellite imagery. *Wea. Forecasting,* **22,** 287–298, doi:10.1175/WAF975.1.

Pfister, L., and Coauthors, 1993: Gravity waves generated by a tropical cyclone during the STEP tropical field program: A case study. *J. Geophys. Res.,* **98,** 8611–8638, doi:10.1029/92JD01679.

Randall, D. A., Harshvardhan, and D. A. Dazlich, 1991: Diurnal variability of the hydrologic cycle in a general circulation model. *J. Atmos. Sci.,* **48,** 40–62, doi:10.1175/1520-0469(1991)048<0040:DVOTHC>2.0.CO;2.

Rogers, R. F., S. Lorsolo, P. Reasor, J. Gamache, and F. Marks, 2012: Multiscale analysis of tropical cyclone kinematic structure from airborne Doppler radar composites. *Mon. Wea. Rev.,* **140,** 77–99, doi:10.1175/MWR-D-10-05075.1.

Tripoli, G. J., and W. R. Cotton, 1989: Numerical study of an observed orogenic mesoscale convective system. Part I: Simulated genesis and comparison with observations. *Mon. Wea. Rev.,* **117,** 273–304, doi:10.1175/1520-0493(1989)117<0273:NSOAOO>2.0.CO;2.

Velden, C. S., and Coauthors, 2006: The Dvorak tropical cyclone intensity estimation technique: A satellite-based method that has endured for over 30 years. *Bull. Amer. Meteor. Soc.,* **87,** 1195–1210, doi:10.1175/BAMS-87-9-1195.

Weickmann, H. K., A. B. Long, and L. R. Hoxit, 1977: Some examples of rapidly growing oceanic cumulonimbus clouds. *Mon. Wea. Rev.,* **105,** 469–476, doi:10.1175/1520-0493(1977)105<0469:SEORGO>2.0.CO;2.

Yang, G., and J. Slingo, 2001: The diurnal cycle in the tropics. *Mon. Wea. Rev.,* **129,** 784–801, doi:10.1175/1520-0493(2001)129<0784:TDCITT>2.0.CO;2.